

PHOTOGRAMMETRY AND LASER ALTIMETRY

Toni Schenk

Department of Civil and Environmental Engineering and Geodetic Science, OSU
schenk.2@osu.edu

KEY WORDS: Photogrammetry, Laser Ranging, DTM generation, Surface Reconstruction, Calibration, Segmentation, Fusion

ABSTRACT

Laser altimetry has, and is continuing to have a profound impact on photogrammetry. This paper discusses the interrelationship between the two fields, identifies problems, and suggests a common research agenda. Surface reconstruction is an important application in photogrammetry. DTMs, for example, are as much an end result as an intermediate step for orthophoto generation and for object recognition. The quality control is a central issue, regardless how the surface is obtained. The paper analyzes the effect of systematic errors of laser ranging systems on the reconstructed surface. To keep these effects as small as possible, rigorous calibration methods are necessary, including suitable test surfaces and proper error modeling. In a more complex setting, better results are achieved if laser ranging is combined with stereopsis. The combination of different surface measurements is a challenging fusion problem. At the sensor level, the systems, such as camera and laser, can be tightly integrated to the degree that the laser footprint is recorded by the camera. On the feature level, extracted features from imagery and laser ranging must be combined in a way that accounts for the different error models. Finally, on the symbolic level, a combined surface must explain the measurements resulting from the different sources.

1 Introduction

Photogrammetry and airborne laser ranging (ALR) are the two most widely used methods for generating digital terrain (DTMs) and surface models (DSMs). Surfaces play an important role in photogrammetry. A DTM is as much an end result as an intermediate step for orthophoto production and object recognition.

The development of airborne laser ranging started in the 1970s in North America mainly for bathymetric applications. With the emergence of GPS and INS other applications, such as monitoring ice sheets in Greenland and measuring canopy heights were successfully approached. As a result, a "laser altimetry" community emerged in North America with researchers from NASA forming the nucleus, and photogrammetrists being virtually absent—quite in contrast to Europe where photogrammetrists greatly facilitated the application of airborne laser ranging.

The present workshop *Mapping Surface Structure and Topography by Airborne and Spaceborne Lasers* is unique in that it brings together for the first time the laser ranging and photogrammetry community—undoubtedly, for the benefit of both. This paper discusses the interrelationship between the two fields, identifies problems and suggests a common research agenda.

The paper begins with a comparison of photogrammetry and laser ranging with respect to generating DTMs. Such comparisons have been carried out in the past, see, e.g. *Ackermann* (1999) and *Baltsavias* (1999) for an extensive review. Here, we emphasize similarities and important differences for the motivation of a joint research agenda. The comparison is divided into data acquisition and surface reconstruction.

Some effort is placed on the impact of systematic er-

rors on the reconstruction of surfaces from laser ranging. This is an important issue because laser ranging does not provide redundant information for the computation of 3-D points. Whether a point is correct or not can only be inferred later—if at all. The quality of laser surfaces depends a great deal on a well calibrated system, including the identification of systematic errors.

The raw laser data forms a cloud of 3-D points that have no topological relationship. Surface properties, such as breaklines and abrupt discontinuities in surface normals, must be made explicit. This is an important post-processing task. The remainder of the paper is a brief summary of essential post-processing steps. Details about most aspects appear as separate papers from our research group at OSU. The collaborative work of Byrd Polar Research Center's Ice Dynamic Laboratory, headed by B. Csathó, and the digital photogrammetry laboratory are a most rewarding experience. We hope that this example encourages further contacts between the laser and photogrammetry community in North America.

2 Comparison between Photogrammetry and Laser Ranging

Photogrammetry and airborne laser ranging (ALR) are the two most popular methods for generating digital terrain models (DTMs) or digital surface models (DSMs) of extended areas. Hence it stands to reason to compare the two methods. This section elucidates similarities and relevant differences. In the interest of brevity we keep the comparison on a general level here. *Ackermann* (1999) and *Baltsavias* (1999) provide more detailed analysis, for example. Table 1 contains a number of comparison factors that are divided into data acquisition and surface reconstruction.

Table 1: Comparison between ALR and photogrammetry.

	photogrammetry	laser ranging
data acquisition		
flying height H	< 6000 m	< 1000 m
swath	< 108°	< 40°
coverage	continuous	irregular
footprint size	$15 \mu\text{m} \times H/f$	$1 \text{ mrad} \times H$
flying time	1 hour	3 to 5 hrs
weather cond.	very restrictive	flexible
surface reconstruction		
redundancy	$2 \times \text{photo} - 3$	0
accuracy		
planimetry	< $15 \mu\text{m} \times H/f$	$1 \text{ dm} + 5'' \times H$
elevation	$\approx H/10,000 \text{ m}$	$\approx 1 \text{ dm}$
surface charact.	explicit	implicit
automation		
degree	medium	high
complexity	medium	low

2.1 Data Acquisition

Essentially, both methods sample the surface. The flying height of existing ALR systems—typically less than 1000 m—is quite limited, compared to photogrammetry. The sampling size (ground pixel size in case of photogrammetry, footprint size in case of ALS) is considerably smaller in photogrammetry when the same flying height is assumed. For $H = 1000 \text{ m}$ and $f = 0.15 \text{ m}$ we have a pixel size on the ground of 15 cm, but a footprint size of 1 m, for example. In ALR systems the average distance between samples is several times larger than the footprint size, resulting in an irregular sampling pattern with gaps. On the other hand, photogrammetry provides continuous ground coverage.

The smaller swath angle of laser scanning systems and the limited flying height cause much longer flying times for covering the same area. *Baltsavias* (1999) mentions a factor of three to five. Since the initial equipment cost and the shorter life time result in substantially higher amortization cost, the data acquisition with ALR is quite a bit more expensive. Now, this is partially compensated by the much less stringent weather conditions for ALR missions; the waiting time for crew and equipment is certainly much longer in photogrammetry.

Another interesting aspect in this comparison is the surface characteristic. It is clear that photogrammetric surface reconstruction methods require a reasonable image function, that is, good contrast or texture. Sand, snow, ice, or water bodies defy photogrammetric methods. Interestingly enough, ALR works very well in these conditions.

2.2 Surface Reconstruction

In this section we briefly compare ALR and photogrammetry in terms of surface reconstruction. Fig. 1 illustrates the principle of determining a surface point by ALR. Although grossly simplified, it captures the basic notion of establishing relationships between different coordinate systems. Let us begin with what we may call the laser beam coordinate system (x', y', z') whose ori-

gin is at the center of the laser's firing point and whose z' -axis is oriented opposite to the direction of the laser beam. In this system, point P on the surface is expressed by the range vector $\mathbf{r} = [0, 0, r]^T$ with r the measured distance (range).

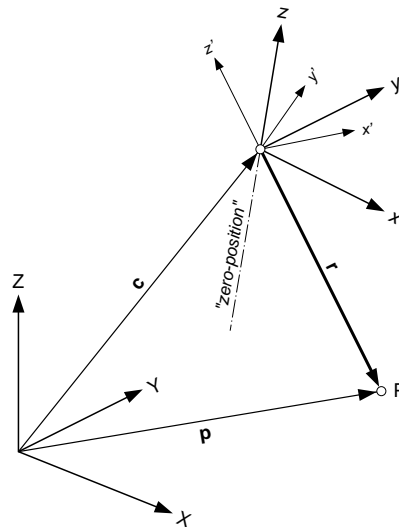


Figure 1: Relationship of local laser coordinate systems and object space reference system for transforming range data to surface points.

Obviously, the laser beam system changes with every new range measured. Let us transform it into the laser reference system, denoted by x, y, z . Its origin is also at the laser's firing point. The orientation depends on the particular system; for example, in nutating mirror systems, the z -axis would be collinear with the rotation axis and the x -axis points to the starting position of the rotating mirror; in the case of a scanning system, the $x-z$ plane would be identical to the scan plane with z indicating scan angle zero.

The transformation from the beam system to the reference system is accomplished by the rotation matrix \mathbf{R}_i since there is only a rotation involved. \mathbf{R}_i is determined by the laser system. In the case of a profiler, \mathbf{R}_i is the identity matrix; for a scanning system, the rotation matrix is determined by the scan angle; two angles are necessary to determine \mathbf{R}_i for a nutating mirror system. Let us call the relationship of an individual laser beam with respect to the reference system the interior orientation of the laser system.

To establish a relationship of the laser system to the object space, the exterior orientation is required. Thus, we obtain for the position of the center of the laser footprint

$$\mathbf{p} = \mathbf{c} + \mathbf{R}_e \mathbf{R}_i \mathbf{r} \quad (1)$$

In this equation, \mathbf{c} expresses the positional and \mathbf{R}_e the angular component (attitude) of the exterior orientation (see also Fig. 1). These two components are usually obtained from GPS and inertial measurements. We omit here the details of establishing the relationship between the platform orientation system and the laser system

for it does not offer new insight into the comparison laser/photogrammetry reconstruction.

Eq. 1 expresses the basic reconstruction principle for laser systems. Note that there is no redundant information for \mathbf{p} ; if the range or the orientation is wrong we will find out—if at all—only later by analyzing local properties of the reconstructed surface.

We now turn to the reconstruction of surfaces by photogrammetry. Fig. 2 illustrates the concept. To compare it as closely as possible to the case just discussed, let us begin with a local image coordinate system (x', y', z') that has its origin at the perspective center. Its z' -axis is collinear to the light ray from the surface point P through the perspective center. In this system, point P on the surface is simply obtained by

$$\mathbf{r} = \lambda \mathbf{d} \quad (2)$$

with $\mathbf{d} = [0, 0, d]^T$ the point vector of image P in the local image coordinate system; λ is a scale factor. Since λ is unknown, it is not possible to determine P from a single image. The standard photogrammetric procedure is to perform the reconstruction from multiple images.

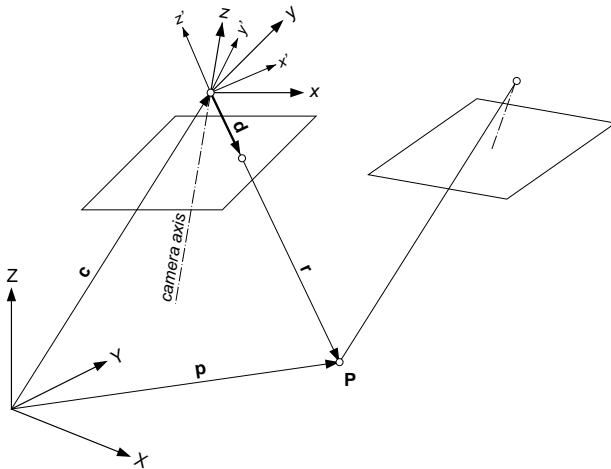


Figure 2: Relationship of local image coordinate systems and object space reference system for reconstructing surfaces from images.

As discussed in the case of the laser system, the local coordinate system changes from point to point. Let us introduce a reference system, known as image or photo coordinate system. The origin is the same, but the z -axis is collinear with the camera axis. The transformation from the local ray system to the reference system is obtained by the rotation matrix \mathbf{R}_i which is defined by the spatial direction of the image vector $\mathbf{r} = [x, y, -f]^T$. Introducing the exterior orientation $(\mathbf{c}, \mathbf{R}_e)$, we find for the reconstruction of P

$$\mathbf{p} = \mathbf{c} + \lambda \mathbf{R}_e \mathbf{R}_i \mathbf{d} \quad (3)$$

This equation is identical to Eq. 1, except for the unknown scale factor λ . The reconstruction from photogrammetry requires two or more images. This is

clearly a disadvantage compared to ALR, because working with multiple images requires that object point P is identified on all images involved. This task—known as image matching—is not trivial if performed automatically. On the other hand, the reconstruction is redundant; each additional image increases the redundancy by two.

To complete the comparison of determining surface points by ALR or photogrammetry, let us briefly discuss how the exterior orientation is obtained. In photogrammetry, two possibilities exist. In the case of direct orientation, the relevant parameters are derived from GPS/INS observations, just as in ALR systems. The traditional approach, however, is to compute the orientation parameters from known features in object space, such as control points. There are two important differences between these approaches. If the exterior orientation is computed from control points then the reconstruction of new points in the object space becomes essentially an interpolation problem. In the case of direct orientation (no control points in object space), the reconstruction resembles extrapolation. Why is this important? Extrapolation has a much worse error propagation than interpolation. Another subtle difference is related to the interior orientation, here symbolically expressed by \mathbf{R}_i . Schenk (1999) points out that errors in the interior orientation are partially compensated in the indirect orientation, but fully affect the reconstruction in the direct orientation.

3 Analysis of Systematic Errors

As discussed in the previous section, the computation of 3-D positions from range measurement and GPS/INS observations is not redundant. If one of the variables in Eq. 1 is wrong we will not find out, except perhaps later when analyzing the data. Thus, it is important to consider the effect of systematic errors of a ALR system on the reconstructed surface—the purpose of this section. As illustrated in Fig. 3, we assume two systematic errors; a positional error \mathbf{q} and an attitude error, expressed by the two angles ω and φ which determine the rotation matrix \mathbf{R}_a . Although this is a grossly simplified view it captures the notion of reconstruction errors. A likely source for a systematic positional error is rooted in the problem of accurately synchronizing the GPS clock with laser pulse generator. How significant is this error? Suppose an average velocity of the airplane of 100 m/sec and a timing error of 5 msec. Then, the resulting positional error would be half a meter—clearly something to worry about for low altitude, high precision laser altimetry projects. A typical example of a systematic angular error is the mounting bias.

The airplane and the laser footprint in point A of Fig. 3 illustrate the data acquisition. The reconstruction of point A is affected by the angular error \mathbf{a} and the positional error \mathbf{q} . Thus, the total reconstruction error is

$$\mathbf{a} = \mathbf{R}_a \mathbf{r} \quad (4)$$

$$\mathbf{e} = \mathbf{q} + \mathbf{a} = \mathbf{q} + \mathbf{R}_a \mathbf{r} \quad (5)$$

With Eq. 1 we obtain for the reconstructed point C

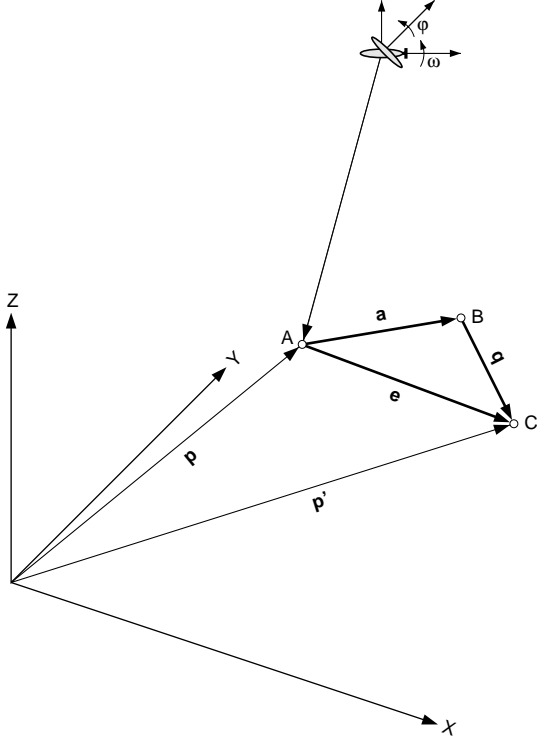


Figure 3: Illustration of a systematic positional and angular error. The angular error causes the footprint in A to be shifted by a to point B . The positional error q translates B to C which is the reconstructed surface point, expressed by point vector p' .

$$p' = p + q + R_d R_e R_i r \quad (6)$$

3.1 Reconstruction Errors Caused by Positional Errors

Profiler and Horizontal Surfaces Fig. 4(a) depicts a laser profiling system during data acquisition over flat ground and a vertical object, say a building. The reconstruction shown in Fig. 4(b) illustrates the effect of a positional error. A timing error, Δt , causes a shift of

$$s = \Delta t \cdot v \quad (7)$$

with v is the velocity of the airplane. Assuming a constant timing error, it appears that its effect is simply a shift of the reconstructed points. This is not quite true as the following analysis reveals.

Fig. 5 illustrates the typical situation where an area is covered by adjacent flight lines, flown in opposite directions. We notice that the shift s in both flight lines is also in opposite direction, causing a distortion of the reconstructed object. Consequently, the reconstructed object space is not simply a translation of the true surface but includes angular distortions, even in the simple case of horizontal surfaces flown by a laser profiling system.

Finally, Fig. 6 shows the relationship between the positional error q and the flight direction. With α the azimuth of the flight trajectory, we have

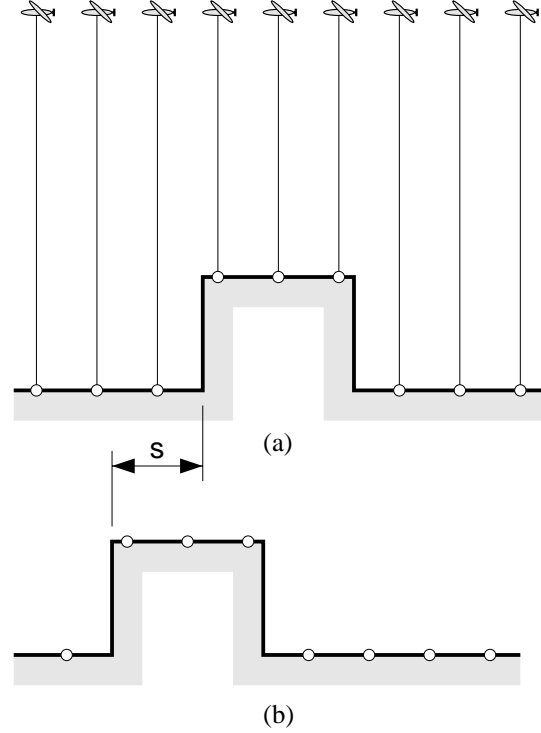


Figure 4: The data acquisition of a laser profiling system is shown in (a). The reconstruction in (b) shows a shift s due to a positional error, caused, for example, by a timing error between GPS clock and laser pulse emission.

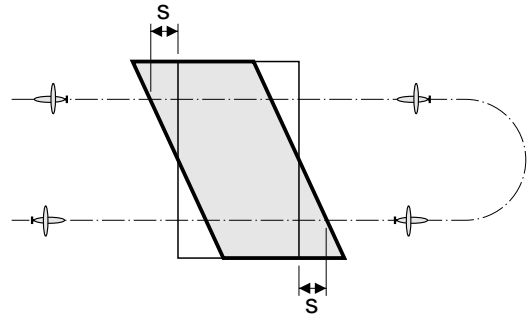


Figure 5: The data acquisition of a laser profiling system shows the typical flight pattern necessary to cover an extended area. The reconstructed rectangular object is distorted, because the shift s is in opposite direction between two adjacent flight lines.

$$q = \begin{bmatrix} q_x \\ q_y \end{bmatrix} = |q| \begin{bmatrix} \sin \alpha \\ \cos \alpha \end{bmatrix} \quad (8)$$

The magnitude in this equation is identical to the shift s of Eq. 7. Eq. 8 demonstrates clearly how different directions of the flight lines affect the reconstruction. Only under the unlikely condition of α being constant is the reconstruction a simple shift. All other data acquisition scenarios will cause angular distortions.

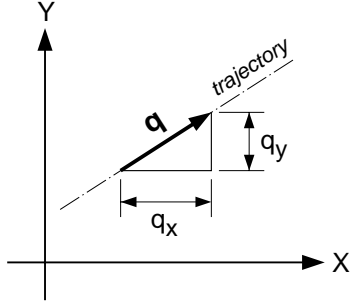


Figure 6: The coordinate components q_x , q_y of the positional error \mathbf{q} are a function of the direction of the flight line, here expressed by the azimuth α .

Profiler and Sloped Surfaces So far we only analyzed the effect of a positional error on horizontal surfaces. Let us now consider sloped surfaces, as illustrated in Fig. 7. As before, a positional error causes a shift of the reconstructed surface. This, in turn, introduces an elevation error that depends on the slope as follows

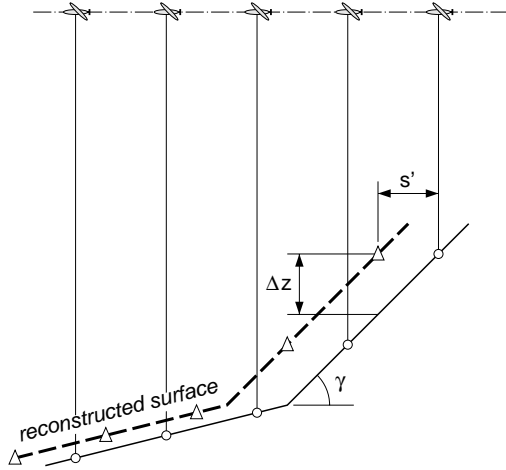


Figure 7: Illustration of the reconstruction error on sloped surfaces. The elevation error Δz depends on the slope angle γ and the shift s' due to the positional error.

$$\Delta z = s' \tan \gamma \quad (9)$$

Here, s' is the shift component parallel to the maximum gradient of the slope. Let α be the azimuth of the flight trajectory and β the azimuth of the slope gradient (see Fig. 8). Then s' can be expressed as a function of these two azimuths. We have

$$s' = |\mathbf{q}| \cos(\beta - \alpha) \quad (10)$$

$$\Delta z = |\mathbf{q}| \cos(\beta - \alpha) \tan(\gamma) \quad (11)$$

An analysis of Eq. 11 reveals that the maximum absolute elevation error is reached if $\cos(\beta - \alpha) = \pm 1$. This confirms our intuition that the error is largest if the flight

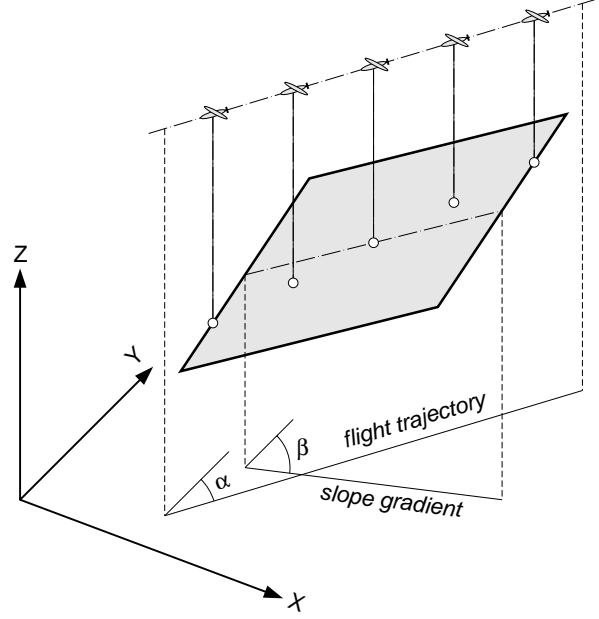


Figure 8: Relationship between the flight trajectory and the slope gradient.

direction follows the maximum slope gradient. Consequently, the elevation error is zero if the flight path is perpendicular to the slope. Moreover, if the flight direction α changes, then an angular error causes a distortion of the surface, even if the slope remains constant.

3.2 Reconstruction Errors Caused by Angular Errors

Let us now investigate the impact of a systematic angular error on the reconstruction of surfaces. An example of an angular error is the mounting bias, see, e.g. *Filin et al.* (1999).

Profiler and Horizontal Surfaces Fig. 9(a) shows a profiling laser system acquiring data over a flat surface and an object, such as building. The reconstruction error a depends on the angle δ and the range r . Assuming that δ remains constant during data acquisition, the magnitude of a changes with the range; the orientation of the error changes with the flight direction.

Because \mathbf{a} , the angular displacement vector, depends on the range, the error is smaller for surface points closer to the laser system. Fig. 9(b) demonstrates the consequence; we realize that the reconstructed flight path is no longer a straight line. The angular error causes a change in the angular relationship of the surface.

Profiler and Sloped Surfaces The next example, depicted in Fig. 10, refers to a profiling system acquiring data on a slope. As the aircraft flies at a constant height in the direction of the maximum gradient, the range gets smaller and smaller. Since the angular displacement vector depends linearly on the range, its magnitude decreases uphill. Consequently, the elevation error also decreases, causing a slope error $\Delta \gamma$ of the reconstructed surface. We find for the slope error the following equation:

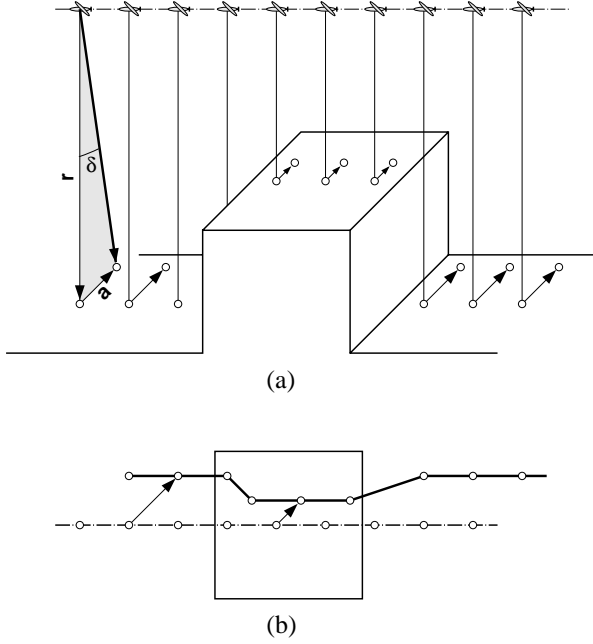


Figure 9: Shown in (a) is a systematic angular error, for example the mounting bias, causing a reconstruction error whose magnitude depends on the range. As a consequence, points that were measured along a straight flight path are unequally displaced, causing an angular distortion in the reconstruction as shown in (b).

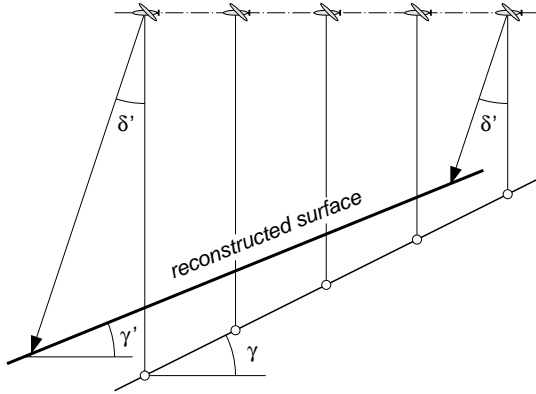


Figure 10: An effective angular error δ' causes an elevation error that decreases as the profiling laser system moves in uphill direction. This causes a slope error $\Delta\gamma$ of the reconstructed surface.

$$\tan \gamma' = \frac{\tan \gamma \cos \delta'}{1 + \tan \gamma \sin \delta'} \quad (12)$$

$$\Delta\gamma = \tan \gamma - \tan \gamma' = \tan \gamma \left(1 - \frac{\cos \delta'}{1 + \tan \gamma \sin \delta'} \right) \quad (13)$$

$$\approx \frac{\tan^2 \gamma \cdot \delta'}{1 + \tan \gamma \cdot \delta'} \quad (14)$$

Eq. 14 is obtained by approximating $\cos \delta' \approx 1$ and $\sin \delta' \approx \delta'$. Considering fairly small angular errors, the

approximation does not introduce noticeable errors.

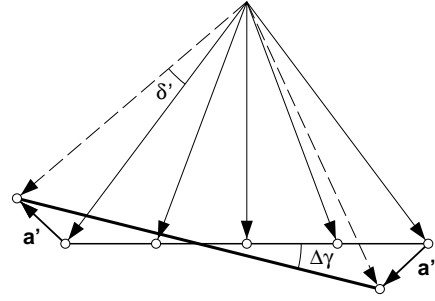


Figure 11: A systematic angular error of δ' introduces a slope error. The reconstructed surface is tilted by $\Delta\gamma$, compared to the true, horizontal surface.

Scanning System and Horizontal Surfaces Let us finally examine the impact of angular errors of a laser scanning system. The first example, shown in Fig. 11, is related to a horizontal surface, flown with a scanning system that has an angular error δ . This error is measured in the plane defined by the range vector and the displacement vector, called error plane here. Fig. 12 depicts the effective angular error δ' . It is obtained by projecting the error plane into the scan plane. Thus, we obtain

$$\delta' = \delta \cos(\epsilon - \tau) \quad (15)$$

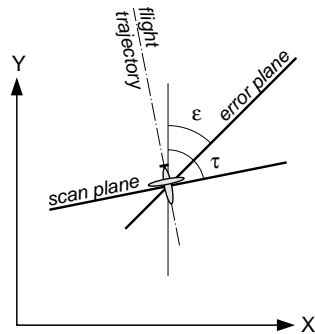


Figure 12: A systematic angular error can be characterized by the angle δ , the angular offset, and the azimuth ϵ of the trace of the error plane. The scan direction is defined by azimuth τ . The effective angular error is the projection of the error plane into the scan plane.

Fig. 11 illustrates the effective angular error δ' causes a displacement vector a' . Its magnitude depends on the range. The shorter the range, the smaller the error. The direction is approximately perpendicular to the range vector. We find for the slope error the following simple relationship

$$\Delta\gamma = \sin \delta' \quad (16)$$

Scanning System and Sloped Surfaces The last example of a systematic angular error is related to a laser scanning system that flies across a tilted surface. Fig. 13(a) depicts this scenario; five individual footprints of one scanning sweep are shown. As in the previous example, the angle δ' indicates the effective angular offset.

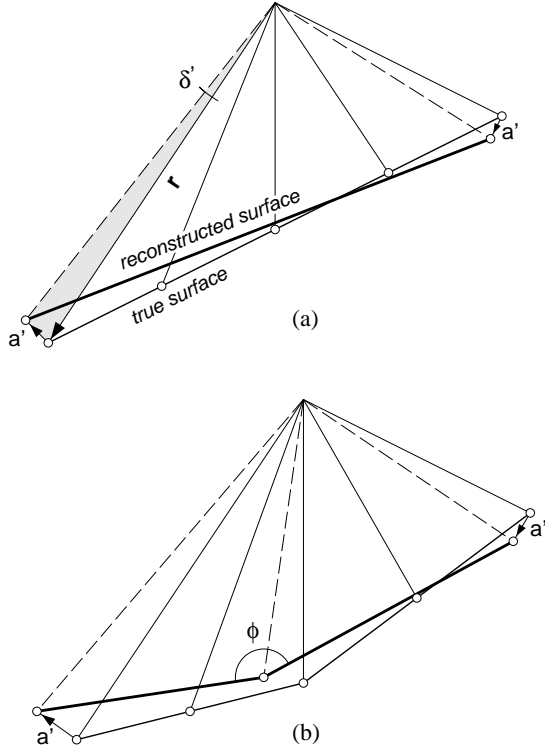


Figure 13: A scanning laser system flies across a tilted surface. Five individual footprints of one scan sweep are shown. The reconstruction is affected by the effective angular error δ' . It causes a displacement of the reconstructed points by an amount that is proportional to the range and δ' . Since the range changes on a tilted surface, the error also changes from point to point. As a consequence, the reconstructed surface has a wrong slope (a). If the slope changes within the swath, the angular relationship between the two slopes, in (b) expressed by ϕ , also changes.

The error a' is a function of the range and the effective angular error δ' . We have

$$a' = |\mathbf{r}| \cos(\epsilon - \tau) \tan(\delta') \quad (17)$$

This error obviously reaches a maximum if $\epsilon = \tau$ which would mean that the angular offset is exactly in the scan plane. On the other hand, the slope error vanishes if the offset is perpendicular to the scan plane.

The magnitude of the error a' depends linearly on the range. Footprints that are closer to the laser system have a smaller error. With the error vectors at both ends of the scan sweep, we can determine the slope error as follows

$$\Delta y = \tan \delta' \tan^2 \gamma \quad (18)$$

3.3 Summary

The simple error analysis in this section demonstrated the effect of systematic positional and angular errors on the reconstructed surface. By and large, the resulting surface errors are a function of the topography, flight direction, and the systematic error. This functional relationship can be exploited to determine the errors if the true surface is known. In the interest of brevity, the error analysis was restricted to profiling and scanning systems. Non-planar scanning systems, such as nutating mirror systems, will show similar effects, but closed-form expressions are more difficult to derive.

The simplest situation involves a profiling system and horizontal surfaces. Intuition tells that causes a horizontal shift that has no influence on the reconstructed surface. The positional error is a vector quantity and as such depends on the flight direction. This, in turn, causes shift errors of variable direction and magnitude. That is, reconstructed horizontal surfaces are distorted. We also recognized that horizontal surfaces, reconstructed from a scanning system with angular errors (mounting bias), have a slope error.

Sloped surfaces present a more complex scenario. Here, the reconstruction error depends on several factors, such as slope gradient, its spatial orientation, flight direction, and systematic positional and/or angular error. In most cases, the errors cause a deformation of the surface. That is, the relationship between the true and the reconstructed surface cannot be described by a simple similarity transformation.

4 Processing and Analyzing Raw Surface Data

Photogrammetry and ALR deliver discrete surface points, called raw surface data in this paper. The cloud of 3-D points is hardly a useful end result. Further processing, such as interpolating the irregularly distributed points to a grid, extracting useful surface properties, and fusing data sets. Moreover, as a quality control measure, the data need to be analyzed for consistency, correctness, and accuracy. We elaborate in the following subsections on some of the post-processing issues with an emphasis on the similarity between data derived from the two methods.

4.1 Calibration

The computation of raw laser data has no internal redundancy. Whether a point is correct or not can only be inferred after processing. For example, systematic errors cannot be detected. The compelling conclusion from the error analysis in the previous section is that systematic errors cause not only elevation errors but also surface deformations. To take advantage of the high accuracy potential of ALR systems, it is imperative to detect and eliminate systematic errors—a process usually referred to as calibration.

In the previous section we have derived some closed form expressions for elevation errors and surface deformations as a function of systematic errors and surface

topography. This suggests to determine the systematic errors based on known deviations of the computed surface. Take Eq. 16, for example. This simple equation permits to compute the effective angular error δ' , such as a mounting bias error. Another example is the determination of a positional error of a profiling system. Eq. 11 can be used to determine the effective positional error s' . However, this would require that we determine elevation differences Δz between the true and the computed surface—a trivial problem at first sight. A closer examination reveals a fundamental problem: how do we compare two surfaces that are represented by irregularly distributed points? Section 4.2 addresses this general problem.

Other challenges of how to calibrate ALR systems loom ahead. Some systematic errors are correlated. For example, one can obtain the same elevation differences or surface deformations either with a positional error or angular error. Imagine the mounting bias error is in the flight direction. Now, the effect of the angular error is very similar to a positional error—the two error sources cannot be separated. The calibration of cameras is also confronted with the same problem. Here, the parameter dependency is solved by choosing a proper calibration surface and decoupling those parameters that are closely correlated. Choosing a suitable topography of the calibration surface is an important issue in calibrating ALR systems. There is no consensus as to what type of surfaces should be used to determine systematic errors and calibration procedures remain ad hoc. Part of the problem is related to the sheer impossibility of identifying the laser footprint on a known surface. Another subtlety is the mathematical model that relates the laser surface to the true surface. As demonstrated in Section 3, most systematic errors cause surface deformations. Consequently, a simple similarity transformation would not properly describe the relationship.

Filin et al. (1999) propose a new calibration scheme that addresses some of the issues raised here and offers solutions. It is a laudable attempt to make laser calibration more transparent and, at the same time, better suitable for quality assessment.

4.2 Comparison of Surfaces

Comparing surfaces is a fundamental, frequently occurring problem when generating DTMs. Calibrating ALR systems is a good example. Here, a known surface is compared with the laser point surface and based on the differences, calibration parameters are determined. An interesting application is change detection where surfaces, determined at different times, are compared in order to identify surface changes that may serve as a basis for volumetric calculations. Merging two or more data sets that describe the same physical surface is yet another standard task. All these cases have in common that the discrete points that describe the same surface are spatially differently distributed, may have different sampling densities and accuracies.

The standard solution is to interpolate the data sets to a common grid followed by comparing the elevations at the grid posts. Although this popular approach is straightforward it is not without problems. For one, the elevations at the grid posts are affected by the interpo-

lation. Moreover, the differences between the two surfaces are expressed along the z – axis which may not be very meaningful for tilted surfaces. Take the extreme example of a vertical surface; Δz values contain no information about how close the surfaces are.

Schenk (1999) describes a surface comparison method that is based on computing differences along surface normals, without interpolating the data sets to a common grid. We present the problem statement, the proposed solution and briefly describe the mathematical model.

Problem Statement Let $S_1 = \{\mathbf{p}_1, \mathbf{p}_2, \dots, \mathbf{p}_n\}$ be a surface described by n discrete points \mathbf{p} that are randomly distributed. Let $S_2 = \{\mathbf{q}_1, \mathbf{q}_2, \dots, \mathbf{q}_m\}$ be a second surface described by m randomly distributed points \mathbf{q} . Suppose that the two sets, in fact, are describing the same surface but in different reference systems. In the absolute orientation problem, set S_2 is the model system and set S_1 is referenced in an object space system. After proper transformation we have $S_1 = S_2$, except for differences due to random errors of the observed points \mathbf{p} and \mathbf{q} . Yet another difference may arise from the discrete representation of the surfaces, for example, $n \neq m$. Even in cases where $n = m$, the different distribution may cause a differently interpolated surface. Suppose further that no points in the two sets are known to be identical (same surface point). The problem is now to establish a transformation between the two sets such that the two surfaces S_1 and S_2 become as similar as possible in terms of closeness and shape.

Solution The problem described is cast as an adjustment problem where the second set of points \mathbf{q} is transformed to the first set such that the differences between the two surfaces are minimized. Additionally, the orientation of surface normals between S_1 and S_2 can also be minimized. Minimizing the distances assures the best positional fit while minimizing differences in surface normals assures the best shape fit.

Mathematical Model Let the points \mathbf{q} be transformed into the coordinate system of the first set by a 3-D similarity transformation

$$\mathbf{q}' = s\mathbf{R}\mathbf{q} - \mathbf{t} \quad (19)$$

The observation equations are defined by the shortest distance from \mathbf{q}' to the surface S_1 . Two scenarios are feasible for expressing surface S_1 . Let us first approximate S_1 in the neighborhood of \mathbf{q}' by a plane, for example by fitting a plane through points \mathbf{p} confined to a small spatial extent (surface patch). Then, the shortest distance d from \mathbf{q}' to the surface patch, expressed in Hessian normal form, using the three directional cosines and the distance p from the origin, is

$$d = \mathbf{q}' \cdot \mathbf{h} - p \quad (20)$$

with $\mathbf{h} = [\cos \alpha, \cos \beta, \cos \gamma]^T$

The following expression is the observation equation for point \mathbf{q}

$$r = (sR\mathbf{q} - \mathbf{t}) \cdot \mathbf{h} - p - d \quad (21)$$

The observation equations are not linear, hence, approximations for the transformation parameters are necessary. *Habib and Schenk* (1999) describe an elegant method of obtaining transformation parameters and surface differences.

If the points \mathbf{p} of the surface patch cannot be satisfactorily approximated by a plane, then a second order surface can be used. Should this also fail, then surface patch is not suitable (not smooth enough) for the proposed procedure and no observation equation is formed for this particular point \mathbf{q} . If it can be sufficiently approximated, then the situation depicted in Fig. 14 applies. The distance from \mathbf{q} to the surface is measured along the surface normal.

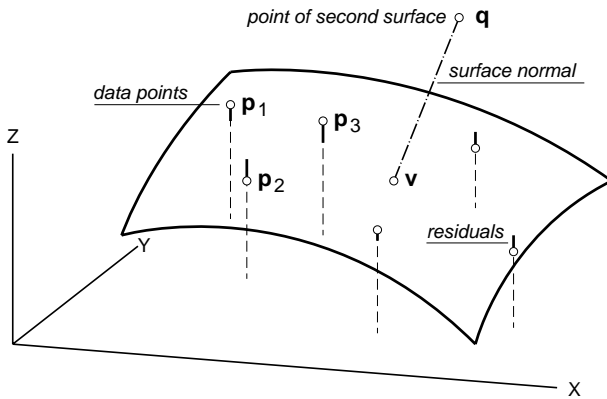


Figure 14: Illustration of determining the shortest distance between point \mathbf{q} and surface patch $SP_{\mathbf{q}}$.

4.3 Post-Processing

The raw 3-D laser point data sets represent physical surfaces in a discrete manner. Because they lack an explicit description of surface properties, meaningful information must be extracted. For most applications, the explicit knowledge of surface properties, such as discontinuities (in elevations and surface normals), piecewise smooth surface patches, and surface roughness, is essential.

Fig. 15 depicts a post-processing schema of raw laser data points. Depending on the application, some or all of the steps are followed. In this paper we have stressed the fact that there is no redundant information available for computing the 3-D position of laser points. On the other hand, the discrete representation of surfaces by randomly distributed laser points is highly redundant. For example, three points suffice to define a planar surface patch, but most likely, hundreds of laser points are available. Statistical blunder detection methods exploit this redundancy. Apart from this traditional methods, there are also reasoning-based approaches for checking the data. Such methods would try to explain the data given the hypothesis of a segmented surface.

Thinning is related to the redundancy of the points. From a practical point of view, thinning is recommended

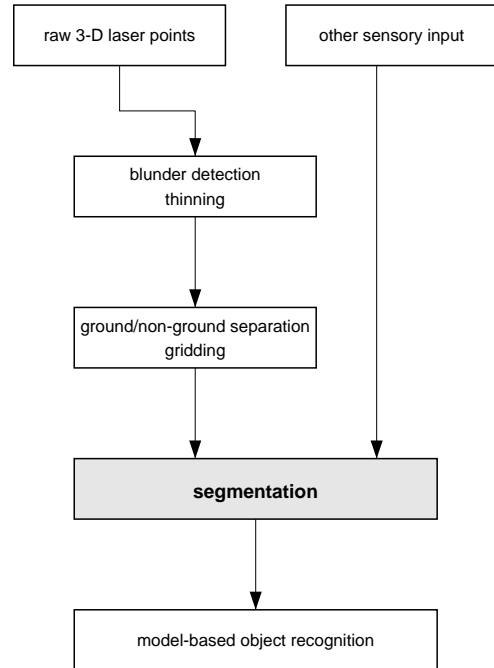


Figure 15: Schematic diagram of the most important post-processing steps of raw laser data sets. By and large, the application determines whether all or even additional steps are necessary.

to reduce the size of the (huge) data sets. Since some points carry more relevant surface information than others, the cardinal question is what points can safely be eliminated. Theoretically, thinning should be treated as a resampling problem with the objective function to minimize the loss of surface information. This, in turn, requires knowledge about the surface topography—a problem that segmentation tries to tackle.

Most every post-processing scheme includes the interpolation of the quasi-randomly distributed laser points to a regular grid (gridding), motivated by the fact that there is a plethora of algorithms available to process gridded data. It is almost equally popular to convert the interpolated elevations at the grid posts to grey levels. The resulting range images are now in a suitable representation for image processing.

Segmentation is the next step in our processing schema. The goal is to make surface properties explicit. Such properties include surface discontinuities (e.g. abrupt elevation changes, abrupt changes of surface normals), piecewise continuous surface patches, and surface roughness. Surface properties are essential in object recognition. As *Csathó et al.* (1999) point out, segmentation is not yet a standard procedure in processing laser data sets. Data thinning and blunder detection, frequently performed in an ad-hoc manner and with proprietary algorithms, is immediately followed by an attempt to detect objects, for example, buildings. It is well known in computer vision that such shortcuts are dangerous. Success with one example does not guarantee generalization of the method.

A more general approach to object recognition requires

additional sensory input, for example imagery. Complementary surface information becomes available from stereopsis. As indicated in the diagram, such information can be merged with laser data in the segmentation process, extending the process to a fusion problem. Csathó *et al.* (1999) present a conceptual framework for including panchromatic, multispectral/hyperspectral imagery, and laser ranging data for the purpose of object recognition and analyzing urban scenes.

5 Concluding Remarks

Photogrammetry and airborne laser ranging are the two most widely used methods for generating DSMs. In some applications, the two methods compete. In this case, the market decides; for example cost, expertise of service providers, availability, project duration. Other applications are clear-cut cases either for laser ranging, such as measuring ice sheets, snow fields, and beaches; or for photogrammetry, for example projects that require imagery for object recognition.

Since the two methods have different performance characteristics, it stands to reason to combine the two methods to solve more challenging problems. Such a combination is facilitated by the possibility of mounting both systems on the same platform. Hence, the data acquisition time does not increase. Perhaps more important, the same GPS/IMU can be used to orient both systems. The ultimate solution in this respect would be an imager that also measures the range, at least of some of the pixels.

The full potential of airborne laser ranging, particularly in combination with photogrammetry, has not nearly been reached. Enthusiasm about the new method is not enough, however. Considerable effort must be devoted to processing the raw laser data. The fair assessment of quality and performance requires transparent processing methods that should be as application independent as possible. Ad-hoc methods should give way for algorithms with a more theoretical underpinning. Some problems look simple at first sight but prove much harder when attempting general and robust solutions. Thinning laser data sets may serve as an example. Most everyone involved with processing laser data developed some sort of thinning algorithm. Do we have a solution that is universally accepted and capable of dealing with profilers and scanners alike? We can compile an impressive list of problems whose efficient solutions require the expertise of different specialists.

A distinct improvement on the system level of laser ranging systems would be the complete recording of the returning signal for the time interval the laser beam interacts with the surface(s). Preliminary studies indicate that additional information about the footprint can be expected—information that is most desirable for solving the difficult object recognition problem.

REFERENCES

Ackermann, F. (1999). Airborne laser scanning—present status and future expectations. *ISPRS Journal of Photogrammetry and Remote Sensing*, 54(2-3), 64–67.

Baltsavias, E. (1999). A comparison between photogram-

metry and laser scanning. *ISPRS Journal of Photogrammetry and Remote Sensing*, 54(2-3), 83–94.

Csathó, B., T. Schenk, D.C. Lee and S. Filin (1999). Inclusion of multispectral data into object recognition. In *International Archives of Photogrammetry and Remote Sensing*, 32(7-4-3W6), 53–60.

Csathó, B., K.L. Boyer and S. Filin (1999). Segmentation of Laser Surfaces. In *International Archives of Photogrammetry and Remote Sensing*, 32(3W2), this proceedings.

Filin, S. and B. Csathó (1999). A novel approach for calibrating satellite laser altimeter systems. In *International Archives of Photogrammetry and Remote Sensing*, 32(3W14), this proceedings.

Habib, A. and T. Schenk (1999). A new approach for matching surfaces from laser scanners and optical sensors. In *International Archives of Photogrammetry and Remote Sensing*, 32(3W14), this proceedings.

Schenk, T. (1999). *Digital Photogrammetry*. Terra-Science, Laurelville, Ohio, 428 p.

Schenk T., B. Csathó and D.C. Lee (1999). Quality control issues of airborne laser ranging data and accuracy study in urban area. In *International Archives of Photogrammetry and Remote Sensing*, 32(3W14), this proceedings.